Radiofrequency Electromagnetic Radiation Exposure Assessment, Analysis, Computation, and Minimization Technique in 5G Networks: A Perspective on QoS Trade-Offs

Adedotun T. Ajibare, Sunday O. Oladejo, Stephen O. Ekwe, Lateef A. Akinyemi, and Daniel Ramotsoela

Abstract—In this study, the specific absorption rate (SAR) and exposure index (EI) of access points (APs) and user equipment (UEs) in fourth-generation (4G) and fifth-generation (5G) wireless technologies are examined with regard to the effects of exposure to radiofrequency (RF) electromagnetic fields (EMF) radiation and the implications of their reduction. We characterize the EI using a classical mathematical method while considering the power density, the SAR, the electric field strength, and the tissue's density and conductivity. As such, a novel exposure-index open-loop power control algorithm is proposed to evaluate the realistic RF-EMF radiation exposure on human users from both the downlink (DL) and uplink (UL) communication devices. To solve an EI minimization problem using the open-loop power control algorithm, we formulate it in the form of a mixed-integer nonlinear programming (MINLP) problem. As the energy capacity (i.e., power density) in wireless networks determines the radiation exposure (SAR and EI), it minimizes the EI by controlling and managing the transmitted and received powers under the restrictions of Quality of Service (QoS), interference, and power, while ensuring the users' QoS requirements are met. Our proposed scheme is numerically compared to other heuristic algorithms and exposure limits established by the International Commission on Non-Ionizing Radiation Protection (ICNIRP) and other similar organizations. Lastly, we compare the emissions from 4G and 5G networks to the emissions from UL and DL transmissions. Our simulation findings indicate that our proposed technique is a good alternative. Our assessment, in terms of numerical results and evaluation, also verifies that the exposures are bearable, fall within the recommended limits, and are minimized without impairing the users' QoS.

Index Terms—RF radiation, 5G networks, power control, MINLP, specific absorption rate, exposure index.

I. INTRODUCTION

A. Background

A.T. Ajibare is with the Department of Electrical Engineering, University of Cape Town, Cape Town, and the NewBridge Graduate Institute, Cape Town, South Africa (e-mail: ajbade004@myuct.ac.za).

S.O. Oladejo is with the School for Data Science and Computational Thinking, Stellenbosch University, Stellenbosch (e-mail: sunday@sun.ac.za).

S.O. Ekwe is with the Department of Electrical Engineering, University of Cape Town, Cape Town(e-mail: ekwste001@myuct.ac.za).

L.A. Akinyemi is with the Department of Electronic and Computer Engineering, Faculty of Engineering, Lagos State University, Lagos, Nigeria and Departments of Computer Science and Electrical Engineering, Schools of Computing and Engineering, College of Science, Engineering and Technology, University of South Africa, Johannesburg, South Africa(e-mail: lateef.akinyemi@lasu.edu.ng).

D. Ramotsoela is with the Department of Electrical Engineering, University of Cape Town, Cape Town, South Africa (e-mail: daniel.ramotsoela@uct.ac.za).

RECENTLY, there has been a proliferation of user equipment (UE) for communication purposes [1]–[3]. The gains in high-throughput, low latency, high QoS, massive connections, and high reliability in 4G and 5G mobile communications [4], [5] have occasioned wireless entry points (or simply put access points (APs)) and a fixed transceiver/base stations (BSs) being installed at an increased rate [6]. With the advent of 5G networks, it is expected that the operating frequency could extend into the millimeter wave band range (i.e., $28\,\mathrm{GHz}$ – $39\,\mathrm{GHz}$) to meet the extreme bandwidth requirements of uses such as online games, high-quality streaming media, and interactive gaming. However, such high operating frequencies cause APs or BSs to have smaller coverage footprints, which results in the densification of access points.

Consequently, there have been rising health concerns in several works of literature about the Radio Frequency (RF)-Electromagnetic Field (EMF) in mobile networks [7]–[10]. Health experts are alarmed by the rise in UEs and radiation exposure to humans. Our work examines how exposure to EMFs from mobile communications affects people. Understanding EMFs in the context of mobile communications is crucial to achieving this.

The emission and transmission of energy through a medium, matter, or space, is the simplest definition of radiation. The transfer of energy packets (i.e., photons with electrical and magnetic properties) at a constant speed is referred to as 'electromagnetic radiation' (EM) [11]. EM radiation exposure can be broadly categorized as either [7]: (i) Ionizing, or (ii) Non-ionizing. Ionizing radiations cause reactions in and damage to the chemical structures of biological tissues (i.e., living cells) owing to the freeing of energized electrons from a living cell's atom [7], [12]. Ionizing radiations have extremely short wavelengths with frequencies ranging between $10^{16}\,\mathrm{Hz}$ – $10^{21}\,\mathrm{Hz}$. They include x-rays, gamma rays, and the upper frequencies of ultraviolet (UV) rays, otherwise known as 'extreme ultraviolet' (EUV). Although ionizing radiations are not visible to the eyes, exposure to them can be cancerous to living tissues, alter DNA structures, and lead to premature death. Figure 1 illustrates the frequency ranges, categories, and wavelengths, respectively, of the EM spectrum.

Non-ionizing radiations do not possess sufficient energy to liberate an electron from a living cell's atom, though their energy is sufficient to produce excitation [7], [13]. Therefore,

they may not result in severely harmful effects on body tissue. Non-ionizing radiations are characterized by very low frequencies in the range $0 - 10^{14}$Hz and include radio waves, microwaves, infrared, visible light, and ultraviolet. The energy levels of ionizing radiations fall between 4.1×10^{-6}eV and 1.2×10^{-3}eV, which is below the minimum energy threshold (i.e., 5eV) of ionizing radiations. There are growing worries about the dangers mobile communication devices and APs pose to the public's health and safety, even though the operating frequencies of mobile communication systems (MCS) do fall into the categories of radio waves and microwaves, which do not pose a serious risk. This paper addresses radiation exposure caused by the MCS, focusing on non-ionizing radiations.

Metrics such as the Exposure Index (EI), Specific Absorption Rate (SAR), EMF strength, and Power Density (PD) have been employed in measuring the levels of radiation exposure to RF-EMF sources [14]–[17]. The SAR measures levels of EMF radiated energy absorbed by the human body when exposed to radiation sources such as cell phones, tablets, and other mobile UEs [9], [18]. To further express the SAR measure in the living tissue, it is characterized as either the [7], [9]: (i) whole body averaged SAR, or (ii) organ-specific SAR, which is local to a part of the body, such as the brain [19]. The closer the EMF source is to the body, the higher the SAR [18], [19].

Unlike the SAR, which addresses EMF radiation exposure for near-field sources, PD is the metric employed to determine radiation exposure to a far-field source. PD is employed when investigating EMFs operating at high frequencies such that temperatures rise and heating is lost to the environment [7]. The EI is the global EMF radiation exposure level of a population of mobile users under a defined network coverage footprint and over a specific time duration [11], [17], [20]. It entails the aggregation of radiation exposures of individuals in a defined area to an EMF source; in our case, the AP or base stations. Additionally, the EI takes into consideration the contribution of the radiation exposure caused by UEs.

A magnetic and electric component make up an EMF produced by an RF source. The amount of current and the potential difference directly correlate with the EMF's intensity.

To reiterate, this work does not address network mobility. However, it should be noted that mobile network handover [21] can significantly impact SAR. When a mobile device switches between networks, there can be a sudden surge in the amount of RF energy emitted, leading to a higher SAR value. Furthermore, frequent network switching can result in a cumulative effect that increases SAR values over time. Therefore, it is essential to set devices at the lowest power level possible to minimize SAR. In addition, switching between different mobile networks (vertical handover) may require more RF energy to establish and maintain a connection, leading to higher SAR levels.

B. Contributions

To assess and determine the specific absorption rate and the exposure index, we calculate the user-to-AP distances d [m], the APs' effectual antenna gains G [dBi], the user-to-serving AP path losses PL dBm, the electric field strengths [V/m], spectral power densities [W/m²], effective isotropically radiated powers measured in [dBm], magnetic field strengths measured in [A/m], the cross-sectional areas [m²] and transmit and receive powers with open-loop control measured in dBm, and notationally and symbolically denoted by E, S, EIRPs, H, CSA, Ptx, and Prx, respectively.

To analyze the radiation exposure caused by wireless networks via simulating the various 4G and 5G network systems, the data obtained by the generated RF-EMF exposure of the given area must be defined. This study, in contradiction to other studies, takes into account computational data to assess and analyze RF-EMF exposure emanating from portable devices, that is, uplink (UL), and broadcasting access points, that is, downlink (DL). The following is a summary of the paper's main contributions.

- We consider the SAR and EI in a multi-cell 5G network. To reduce the network's overall EI, an optimization problem known as 'EI minimization' is devised. This system effectively reduces customers' radiation exposure while ensuring the required Quality of Service (QoS) is met and maximum interference is not exceeded. In minimizing the EI, network parameters such as transmit power, data rate threshold, base station height, cell coverage radius, and human-body characteristics such as conductivity and mass density are taken into consideration.

- As stated, the EI minimization issue is expressed as an optimization mixed-integer nonlinear programming (MINLP) problem. We exploit the idea of the Fractional Power Open Loop Control (FPOLC) algorithm in optimizing the EI minimization framework. For uplink transmission, the FPOLC regulates the UE's transmit power. An EI-based Power Control Algorithm is proposed, which takes into consideration the network and human-body parameters stated in the previous bullet point.

- A straightforward propagation model is used to derive the mathematical expressions for the EMF exposure metric, which takes into account network characteristics including the path loss exponent, transmit power, electric field strength, characteristic impedance, antenna efficiency, and antenna directivity.

- Through comprehensive simulations, we show the effectiveness of the suggested EI minimization framework. Different scenarios' performances are taken into account. Additionally, we look at the EI exposure for both the more current 5G gNB and users as well as 4G eNB and users.

C. Organization

This paper is ordered as follows: Section II gives a detailed summary of related works. The system model is thoroughly described in Section III. The global EI minimization problem is formulated as a resource allocation optimization problem in Section IV. In Section V, the proposed solutions are discussed. Section VI presents and discusses the simulation results. Finally, our conclusion is drawn in Section VII.
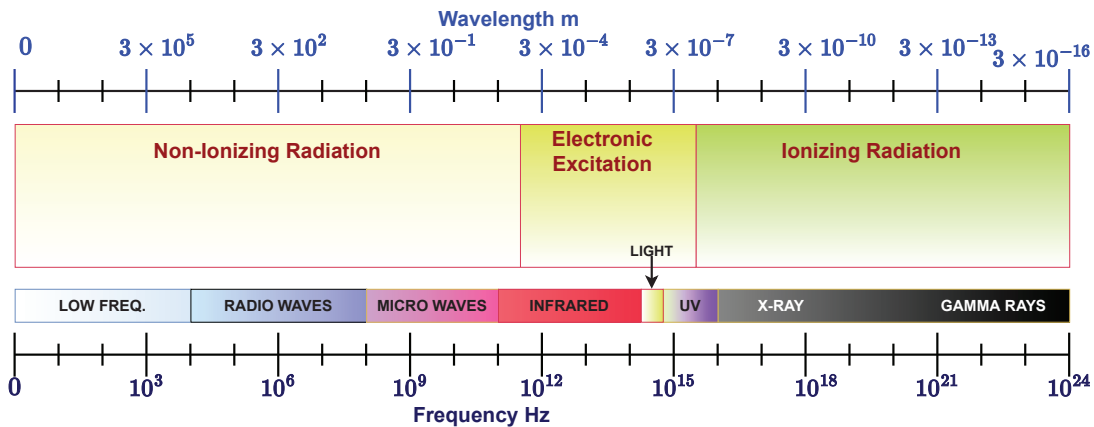
Fig. 1. Illustration of the EM spectrum.

II. RELATED WORKS

Network infrastructure and services in densely populated urban cities are made sustainably smart (especially the antenna design) to make the environment more friendly, inhabitable, and safe [22], [23]. In the literature, several works such as [24]–[29] have considered 5G networks' QoS from a resource allocation perspective, but did not address RF-EMF radiation. The authors in [30] explore a step-by-step resource allocation method for optimizing resources in massive MIMO-OFDMA DL systems. They used the calculated bandwidth of each user to allocate the power and the number of access point antennas. The average signal-to-noise ratio and bit rate received by the user are set as parameters to allocate resources in the proposed multi-user MIMO energy efficiency water injection algorithm. Rising health concerns [31], [32] in the literature on RF exposure due to mobile networks' operation make it imperative to consider this factor in the design of mobile networks.

The work in [33] generated a brief overview of RF-EMF radiation EI in 5G networks. The author raised critical questions that serve as research challenges and bridge the knowledge gap concerning 5G's RF-EMF radiation exposure's effect on body tissues. Furthermore, the works in [34]–[37], among others, concentrated on the effects of RF exposure on the human brain. Specifically, the authors addressed the exposure caused by UL transmission. They did not address the RF exposure due to DL transmission, and therefore a global RF exposure was not captured in the works.

In [38], the authors proposed a simplified method for determining a population's RF's EI in an LTE network situated in an urban area. The proposed method is premised on surrogate modeling for daily global population EI estimates, considering both the UL and DL transmission. The surrogate method, which helps to reduce computational complexity and time, employs Polynomial Chaos Expansion (PCE), which relies on Least Angle Regression Selection (LARS). The proposed method considered network parameters such as propagation path loss, network utilization, and throughput. The authors considered the sensitivity analysis of the network parameters. However, the authors did not consider the SAR of the 5G networks. Additionally, they did not address the evaluation of the EI metric.

The authors of [39] carried out RF radiation exposure level measurement tests in locations in Dar es Salam, Tanzania, for mobile networks in 900MHz and 1800MHz (i.e., GSM), and 2100MHz (i.e., UMTS) frequency bands, based on the International Commission for Non-Ionizing Radiation Protection (ICNIRP) guidelines [15]. The parameters measured in [39] were the power density, and electric and magnetic fields, respectively, with the aid of a selective radiation meter (i.e., SRM 3006 tool). The authors did not consider the radiation measurement due to the UL transmission. Moreover, the authors in [39] did not address global radiation exposure metrics, such as the SAR and EI. They also did not consider the 5G network, which has peculiar network parameters and configurations such as higher operating frequencies and high network density.

Unlike [39], the work in [40] considered the measurement of radiation exposure in 5G networks with frequencies in the range 800MHz-3600MHz. It took into account both UL and DL radiations. In [40], the authors carried out RF radiation measurement tests for both the base station transmissions (i.e., DL) and UL transmissions (i.e., uplink from a handheld device) in an area with poor network signal reception. The authors carried out the test for a few days. As previously stated, notationally, E [V/m], H [A/m], and SAR are the metrics measured for DL and UL communication devices. The authors in [40] did discuss the average measurement time for each day. They did not consider the global EI and a multicell network scenario.

The authors in [41] investigated the impact of various transmit powers of 4G UE on RF radiation exposures in rural, suburban, urban, and indoor environments, respectively. Unlike in [40], the authors in [41] considered a multicell network scenario comprising a total of 41 evolved nodal base stations (eNodeB) with 235 LTE cells, serving about 7000 UEs. Two of the critical network parameters measured were the power headroom [42] and UL transport time. To this end, the authors derived the time-averaged output power [43] from the measurements from power headroom reports (i.e., UE's output power) and the UL transport time (i.e., UE UL transmission time). However, in [41], the authors only

addressed RF radiation emanating from the UL transmission in a 4G network. The authors demonstrated how crucial actual UE and eNodeB power levels were for a proper assessment of RF-EMF exposure.

The SAR characteristics of a planar inverted-F antenna (PIFA) were the subject of a study that was presented in [44]. In this work, the impact of the positioning and antenna's number in the mobile device is explored. Different scenarios were presented, analyzing the positioning of the user equipment when put next to a standard specific anthropomorphic mannequin (SAM) head. The authors noted the device's deterioration and users' average SAR readings being higher than the users with antennas positioned at the mobile devices' upper part.

An optimization framework for the minimization of the radiation exposure from APs and UEs in indoor environments was proposed in [45]. The authors suggested a Genetic Algorithm (GA) optimization technique coupled with site-specific ray-tracing approximation for the prediction and minimization of the Safety Index (SI).

The authors in [46] propose an EMF-aware resource scheduling method that leverages power domain non-orthogonal multiple access (PD-NOMA) and unsupervised machine learning (ML). It controls the maximum number of users allocated to the subcarrier per time by intelligently grouping the users into different K-means clusters, and further formulating a convex optimization problem to minimize their exposure.

In [47], the authors evaluated the exposures from RF-EMF in a wireless network and examined the instantaneous association between the transmit and received powers of a mobile device, with the goal of estimating the exposure from the radiating waves by extrapolating the measured powers.

In [48], a smart-city test-bed, which relies on an Internet of Things (IoT) based platform to assess the radiation exposure metric EI across a geographical area, is proposed. The RF exposure map for a city is captured by the placement of several low-complexity dosimeters (i.e., IoTs) for radiation measurements in different locations. The collection, processing, and spatial representation of the respective measurements were employed in the creation of exposure maps. The authors in [48] considered the network scenarios of GSM, UMTS, and WIFI technologies. However, [48] only considered the radiation exposure due to DL transmission. This does not fully reflect the aim and intention of proposing EI, which considers both UL and DL radiation exposures. Moreover, the authors did not consider 5G mobile networks in their work.

In [49], [50], and [51], strategies for minimizing the global exposure from a radiating electromagnetic field were proposed. In [49], the authors explored strategies such as network deployment topology, environments (i.e., network traffic condition), mobile user behavioral characteristics (i.e., mobility), and user profiles (i.e., services subscribed to). The authors in [50] minimized EMF exposure by taking into consideration QoS and network capacity and explored the impact of user distance from the access point and inter-site distance (ISD) on the RF-EMF exposure. It was surmised that the UL EMF exposure improves as the distance between the UEs and APs

decreases. Additionally, the authors in [50] concluded that 5G network APs are in close proximity to the users and that this lowers the transmit power in the UL and, consequently, reduces RF-EMF exposure. To minimize users' SAR exposure while keeping the required QoS, the authors in [51] proposed an offline and online UL strategy in the orthogonal frequency-division multiplexing (OFDM) structures. The offline scheme is a convex optimization problem, solved using the water-filling method, predicated on the notion that all users' long-term channel state information (CSI) is known. The online EM emission reduction technique depends on reducing the energy per bit of each user.

In contrast to previous works, we minimize the global EI of the mobile network in this paper while ensuring that QoS is not compromised. This, we achieve via efficient resource assignment in the network, such as transmit power and resource blocks. Moreover, this paper focuses on UL and DL transmissions to fully capture RF exposure to users.

III. SYSTEM MODEL

The system model and pertinent analytical background are presented in this section. Figure 2 provides an illustration of the system model discussed in this study.
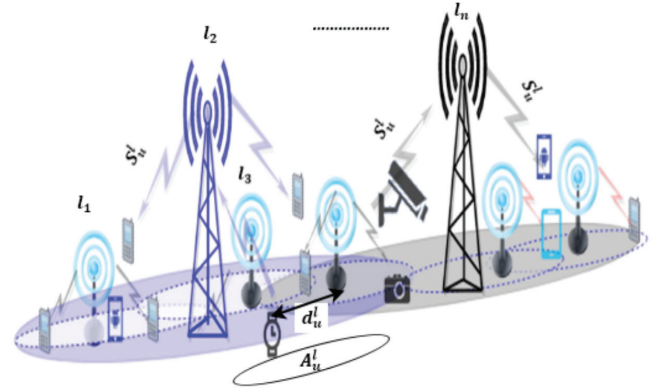

Fig. 2. Illustration of the system model.

A. General Model

The proposed case investigates the conventional dense deployment of base stations and high user density unique to an urban environment. The set of users $\mathcal{U}$ is uniformly distributed across the geographical area A, having radius r. The area A is densely overlaid by APs typical of an urban scenario. The set of APs is defined as $\mathcal{L}$. We focus our discussion around users that are not mobile and also assume a user $u \in \mathcal{U}$ is in the presence of a mobile device (i.e., a handheld gadget) to present a simple and realistic deployment. Consider a user $u \in \mathcal{U}$, under the coverage of an AP $l \in \mathcal{L}$; the distance between $u \in \mathcal{U}$ and $l \in \mathcal{L}$ is defined as d_u^l, and the radiated wave's surface cross-sectional area is denoted by A_u^l.

For a user $u \in \mathcal{U}$ to communicate with an AP $l \in \mathcal{L}$, the UL signaling transmit power on a subcarrier $c \in \mathcal{C}$ is denoted as $P_{u,c,l}^{Tx}$. Similarly, for the AP $l \in \mathcal{L}$ on a subcarrier $c \in \mathcal{C}$,

the signaling received power is given as $P_{u,c,l}^{Rx}$. The set of subcarriers $\mathcal{C}$ is such that the aggregate sum of all subcarriers is approximately equal to the system bandwidth $\mathcal{B}$, in the frequency domain. The size, $b_{u,c}^l$, of a $c \in \mathcal{C}$ depends on the radio access technology. For a 4G AP, $b_{u,c}^l = 180$KHz [52] and $b_{u,c}^l = 360$KHz, depending on the 5G numerology adapted [53].

The carrier frequency of an AP $l \in \mathcal{L}$ is denoted by f_c^l (i.e., in MHz) and the height of $l \in \mathcal{L}$ is represented as h_l.

B. Channel Model

According to the fundamental RF principles, the near-field principle is impacted by electromagnetism (i.e., induction-based), whereas the far-field principle is predicated on electromagnetic waves (i.e., radiation-based). Consequently, users are exposed to EMF radiation when located in the far-field region[1] (i.e., for distances beyond $2K^2/\lambda$).

The radiated wave's surface cross-sectional area, A_u^l, is given as:

$$A_u^l = 4\pi(d_u^l)^2 , \qquad (1)$$

The path loss model in use in this work for the respective users is dependent on the radio access technology and is given [54]–[57] as:

$$\omega_u^l = \begin{cases} 36.8\log_{10}(d_u^l) + 43.8 + 20\log_{10}(f_c^l), & \text{eNB APs} \\[2mm] 32.45 + 20\log_{10}(d_u^l) + 20\log_{10}(f_c^l), & \text{gNB APs,} \end{cases} \qquad (2)$$

where d_u^l, f_c^l, and ω_u^l denote the user's distance $u \in \mathcal{U}$ from an AP $l \in \mathcal{L}$ in metres (m); the carrier frequency of the signaling link in MHz; and the path loss between an AP $l \in \mathcal{L}$ and a user $u \in \mathcal{U}$ in decibels (dB).

C. Radiated Power Modelling

Owing to our interest in radiation exposure, we focus our attention on the isotropic antenna due to its unique properties. An isotropic antenna is characteristically a lossless antenna and has a directivity, D, of 1. Consequently, a power-radiating isotropic antenna emits or transmits throughout all directions symmetrically. The antenna gain, G_T, is given by [57]:

$$G_T = \beta D(\theta, \phi), \qquad (3)$$

The antenna's output power to input power ratio, denoted by β is expressed as a ratio where β denotes the antenna efficiency, which is the antenna's output power to input power ratio. $D(\theta, \phi)$ is the directivity of the antenna, which is a function of (i) the antenna altitude, θ, and (ii) the antenna angle ϕ with respect to the reference plane.

The EIRP [58] expressed in decibels is the resulting gain of the antenna multiplied by the transmit power given in (3). The EIRP is given by [59]:

[1]K is the antenna's largest dimension and λ is carrier frequency's wavelength

$$EIRP(\text{dBm}) = [P_T(\text{dBm}) - Loss(\text{dB})] + G_T(\text{dBi}), \quad (4)$$

where $Loss$ (i.e., body loss) denotes signal attenuation in dB resulting from cable connection between the antenna and transmitter. P_T is the transmitter output power in dBm.

Alternatively,

$$EIRP(\text{W}) = P_T G_T. \qquad (5)$$

From (4) and (5), it can be concluded that the P_T is critical to EIRP evaluation. The ability to control the power is crucial in cognitive radio management to optimize the needed signal power while reducing radiation and interference. Therefore, transmit power in the downlink scenario, which is also the received power of the UE, is given by [60], [61]:

$$P_{u,c,l}^{Rx} = P_0(c) + \alpha \, \omega_u^l, \qquad (6)$$

where $P_0(c)$ is a UE/cell-specific transmit power parameter contained or associated with a subcarrier $c \in$ C. α denotes the path loss compensation factor, where $0 \leq \alpha \leq 1$, with $\alpha = 0$ as a no-power control mode. Fractional power control is when $\alpha > 0$. Lastly, $\alpha = 1$ when there is a full path loss compensation mode.

Similarly, the UL transmit power, $P_{u,c,l}^{Tx}$, is given by [60], [61]:

$$P_{u,c,l}^{Tx} = \min\{P_{max}^{Tx}, \, P_0(c)+\alpha \, \omega_u^l+10\log_{10}(N_u)+\delta+f(\Delta)\}, \qquad (7)$$

where P_{max}^{Tx} denotes the maximum transmit power threshold in the UL mode and is UE-specific. N_u indicates the number of resource blocks allocated to a user $u \in \mathcal{U}$. Moreover, δ and $f(\Delta)$ represent the modulating code scheme's (MCS) offset and closed loop correction function. Owing to how UE's are designed to operate below the maximum transmit power threshold P_{max}^{Tx} and neglecting the variables δ and $f(\Delta)$ in (7), an approximation of $P_{u,c,l}^{Tx}$ is given by [60]:

$$P_{u,c,l}^{Tx} = P_0(c) + \alpha \, \omega_u^l + 10\log_{10}(N_u). \qquad (8)$$

Additionally, combining (1) and (5) yields the spectral power density, S_u^l in (W/m^2), with the closed-form expression given by:

$$S_u^l = \frac{P_T G_T}{4\pi(d_u^l)^2} \qquad (9)$$

S_u^l can be expressed in terms of the electric field strengths, E_u^l, root-mean-square (rms) value and the wave impedance, η_0, as [58]:

$$S_u^l = \frac{\left|E_u^l\right|^2}{\eta_0}, \qquad (10)$$

where η_0 is of the value $120\pi\Omega$. To this end, combining (9) and (10), the electric field strength, E_u^l, can be expressed as:

$$E_u^l = \left(\eta_0 \frac{P_T G_T}{4\pi(d_l^u)^2}\right)^{1/2} \qquad (11)$$

To quantify the radiation absorbed by a tissue, the SAR metric, Ω_u^l, is employed as explained in Section I. The SAR, Ω_u^l, is directly proportional to the electric field strength's root-mean-square value and can be expressed as [62]:

$$\Omega_u^l = \left| E_u^l \right|^2 \left(\frac{\sigma_u}{\rho_u} \right), \tag{12}$$

where ρ_u and σ_u are tissue density in $\mathrm{Kg/m^3}$ and the tissue's electrical conductivity (i.e., in $\mathrm{S/m}$) of the user $u \in \mathcal{U}$, respectively. From (11) and (12), we can simply express Ω_u^l as:

$$\Omega_u^l = \left| \left(\frac{\eta_0 P_T G_T}{4\pi (d_l^u)^2} \right)^{1/2} \right| \left(\frac{\sigma_u}{\rho_u} \right). \tag{13}$$

To conclude this subsection, we explore the EI metric along the lines of the SAR. Since EI is the ratio between the measured SAR for the whole body (or for specific body parts, such as the head) taken in intervals of 30 minutes (or 6 minutes for specific body parts) and the maximum SAR threshold [47], the EI ψ_u^l is expressed as [47]:

$$\psi_u^l = \frac{\Omega_u^l}{\Omega^{max}}, \tag{14}$$

where Ω_u^l is the measured or evaluated SAR, and Ω^{max} denotes the maximum SAR threshold.

D. Power Classes

In wireless communication, 'power class' refers to the highest amount of power a transmitting device can emit, which is generally regulated by national or international governing bodies. These classes can differ depending on the region. In 4G and 5G technologies, standard power classes are used to guarantee compatibility between devices made by various manufacturers. Power classes are established by the 3rd Generation Partnership Project (3GPP), a coalition of telecommunications standards organizations. The 3GPP Technical Specifications 36.101 and 38.101 define the four distinct power classes for UE in 4G LTE and 5G, respectively [63], [64]. In this work, the power class 2 is used for UEs in both 4G LTE and 5G networks, with a maximum output power of 24dBm (250mW), as shown in Table I.

Consequently, the actual power consumption of a UE in 4G and 5G networks can differ based on various factors, such as the network setup, user application, frequency spectrum, distance between UE and base station, and the number of UEs connected to the network. Generally, 5G networks function on higher frequency bands than 4G networks, which results in shorter transmission distances but higher power demand. This is due to the necessity of deploying more base stations and incorporating advanced antenna technologies like massive MIMOs for better coverage and capacity. Nevertheless, technological advancements are helping to decrease the power consumption of 5G networks with the utilization of more effective hardware and software to fulfill the requirements of high-speed data transmission and extensive device connectivity.

IV. PROBLEM FORMULATION

In this section, the global radiation exposure problem in a mobile network is examined. The EMF-RF EI minimization problem is formulated as a resource allocation problem, given in (15). Simply, the objective of the resource allocation problem is to efficiently minimize the mobile network's global EI while meeting QoS requirements such as interference threshold, power budget, bandwidth, and data rate threshold.

$$\max_{P, \; x_{u,c}^l(t)} \sum_{l \in \mathcal{L}} \sum_{u \in \mathcal{U}} \psi_u^l \tag{15}$$

subject to:

$$C1: \quad \sum_{u \in \mathcal{U}} \sum_{c \in \mathcal{C}} x_{u,c}^l(t) \, b_{u,c}^l \leq \mathcal{B}; \quad \forall \, t \in \mathcal{T}, \quad \forall \, l \in \mathcal{L}$$

$$C2: \quad \sum_{u \in \mathcal{U}} \sum_{c \in \mathcal{C}} x_{u,c}^l(t) \, P_{u,c}^l \leq P_u^{max}; \quad \forall \, t \in \mathcal{T}, \quad \forall \, l \in \mathcal{L}$$

$$C3: \quad \sum_{u \in \mathcal{U}} x_{u,c}^l(t) \; \leq 1; \quad \forall \, t \in \mathcal{T}, \quad \forall \, l \in \mathcal{L}$$

$$C4: \quad x_{u,c}^l(t) \sum_{u \in \mathcal{U}} (t) \, I_{u,c}^l(t) \leq I_u^{max}; \quad \forall \, t \in \mathcal{T}, \quad \forall \, l \in \mathcal{L}$$

$$C5: \quad R_u^{min} \leq R_{u,c}^l \quad \forall \, u \in \mathcal{U}, \, \forall \, l \in \mathcal{L}, \, \forall \, c \in \mathcal{C},$$

In (15), $x_{u,c}^l(t)$ denotes the binary resource allocation decision variable of the subcarrier $c \in \mathcal{C}$ in AP $l \in \mathcal{L}$ allocation to user $u \in \mathcal{U}$ at time t.

The constraints in $C1$ to $C5$ ensure that solutions obtained are feasible. Constraint $C1$ ensures that the total bandwidth of an access point is not exceeded. This also ensures that the number of PRBs available on the AP is not exceeded. Moreover, in $C1$, $b_{u,c}^l$ is the size of the allocated subcarriers and $\mathcal{B}$ represents the system bandwidth. Constraint $C2$ describes the limitations associated with the power budget of an AP $l \in \mathcal{L}$. $C2$ ensures the power budget of an access point is not exceeded. $P_{u,c}^l$ is the transmit power of the PRB allocated and P_u^{max} denotes the maximum power threshold. Constraint $C3$ enforces that a user $u \in \mathcal{U}$ is only associated with an access point $l \in \mathcal{L}$ and a subcarrier is uniquely allocated to a single user. Constraint $C4$ is otherwise referred to as the 'interference temperature constraint'. It places a threshold on the interference levels of the network by ensuring that it is not more than the interference limit set. The tolerable interference threshold is denoted as I_u^{max}, and $I_{u,c}^l$ is the interference experienced by each user and is defined as:

$$I_{u,c}^l = \sum_{j=1, j \neq l}^{\mathcal{L}} \sum_{j=1, j \neq u}^{\mathcal{U}} P_{u,c}^l \, |h_{u,c}^l| \, , \tag{16}$$

here $h_{u,c}^l$ is the channel gain of a user u allocated subcarrier c. Constraint $C5$ is the data rate constraint for each UE. This ensures that the QoS is met based on the minimum data SLA, while achieving the objective function in (15). R_u^{min} is the minimum required data rate of each user, whereas $R_{u,c}^l$ is the throughput or the allocated data rate for each user

and its signal-to-interference-plus-noise ratio (SINR), $\gamma_{u,c}^l$, are defined in (17) and (18) as:

$$R_{u,c}^l = x_{u,c}^l \ b_{u,c}^l \ \log_2(1 + \gamma_{u,c}^l) \ , \qquad (17)$$

and

$$\gamma_{u,c}^l = 10\log_{10} \frac{P_{u,c}^l \ |h_{u,c}^l|}{N_0 + \displaystyle\sum_{j=1,j\neq l}^{\mathcal{L}} \sum_{k=1,k\neq u}^{\mathcal{U}} P_{k,c}^j \ |h_{k,c}^j|}, \qquad (18)$$

where N_0 is the noise spectral density.

V. PROPOSED SOLUTION

The proposed algorithm solves the optimization problem in (15). To obtain the SINRs that provide the necessary data rates for each user, a workable power solution is needed. EI is minimized by minimizing the transmit power and the transmit time since EI is a function of transmit power and transmit time. Depending on the service type, use case, and network slice to which the users belong, the network offers the minimum data rate that has been agreed upon for each user. Due to restriction C5, the needed data rate must be met even though the goal is to minimize the transmit power and the transmission time of signals to reduce the user's overall EIs, as stated in (14). Additionally, the total bandwidth restriction established across all PRBs for every network user must be met and the same as in C1. C2 makes sure that the total power budget is under the power limit. Moreover, the interference threshold constraints and the subcarrier binary allocation are satisfied while optimizing the EI, as described in Alg. 1. Using the power control expressions in (6)-(8) in conjunction with the path loss compensation factor (α), the set constraints are evaluated at every MINLP solution. The MINLP problem is solved until all the constraints are satisfied. Hence, the defined objective function is solved until feasibility and optimality are achieved.

The benchmark algorithm is a conventional 5G network power algorithm adapted from [65], where power is equally allocated across all the PRBs, and the pseudo-code is as presented in Alg. 2. The approach is also a resource allocation MINLP optimization problem but with fixed gain to the time-dependent channels. The objective is to minimize the total transmit power subject to power constraints and data rates. The benchmarked algorithm is expected to satisfy all the requirements while optimally achieving this objective. Consequently, all users are assigned more than the required SINR, or data rate, even at worse channel conditions, which increases network challenges such as interference and the RF-EMF exposure of end-users in the networks. Unlike the proposed algorithm, the average throughput of the users might be optimal. However, the network challenges are not (minimized) optimal.

VI. NUMERICAL RESULTS

This section presents the performance evaluation of the proposed EI model carried out via intensive simulations in a MATLAB environment. We considered a mobile network

---

Algorithm 1 EI open-loop power control algorithm

Input: Z_0, P_0, α, $\mathcal{B}$, f_c, λ, h_g, r, D, U, G_T, L, C, d_u
Output: Ω_u^l, $E_{u,c}^l$, $R_{u,c}^l$, $I_{u,c}^l$, ψ_u^l

1: **for** $u \leftarrow 1$ to $|\mathcal{U}|$ **do**
2:     Initialise the data for P_{UE}^{max}, SAR's limits, ρ, and σ
3:     Determine dist. of UEs from interfering Access Points
4:     **if** $\frac{2D^2}{\lambda} \leq d \leq \lambda$ **then**
5:         Evaluate the path loss ω_u^l of UEs using (2)
6:     **else**
7:         User $u \in \mathcal{U}$ is not exposed to the the RF-EMF radiation
8:     **end if**
9:     **for** $l \leftarrow 1$ to $|\mathcal{L}|$ **do**
10:         Initialise the values of P_u^{max}
11:         Determine interfering APs DL transmit power $P_{u,c,l}^{Rx}$ using (6)
12:         **while** $P_{u,c}^l \leq P_u^{max}$ $\forall l \in \mathcal{L}$, $\forall u \in \mathcal{U}$ **do**
13:         $P_{u,c}^l \leq EIRP_{TX}$
14:         **end while**
15:     **end for**
16:     Estimate the CSA of RF wave to the UE u using (1)
17:     Set $I_{u,c}^l = 0$, $t = T$, and $\forall c \in \mathcal{C}$
18:     Determine uplink received power $P_{u,c,l}^{Tx}$ for each UE from interfering APs
19:     **while** $P_{u,c}^l \leq P_u^{max}$ $\forall l \in \mathcal{L}$, $\forall u \in \mathcal{U}$ **do**
20:         $P_{u,c}^l \leq EIRP_{TX}$
21:         $I_{u,c}^l \leq I_u^{max}$
22:         $\sum_{c \in \mathcal{C}} b_{u,c}^l \leq \mathcal{B}$
23:         $R_u^{min} \leq R_{u,c}^l$
24:     **end while**
25:     Using (12), determine the spectral power density $S_{u,c}^l$
26:     Solve for the RMS values
27:     Assume constant values for ρ and σ
28:     Find Ω_u^l using (13)
29:     Solve for the ψ_u^l using (14)
30:     **if** $R_u^{min} \leq R_{u,c}^l$ **then**
31:         Determine ψ_u^l
32:         Terminate if the optimal solution is found
33:     **else**
34:         Increase $P_{u,c}^l$ or set $P_{u,c}^l = P_u^{max}$
35:     **end if**
36: **end for**

Algorithm 2 Conventional 5G network power algorithm [65]

Input: Z_0, P_0, α, $\mathcal{B}$, f_c, λ, h_g, r, D, U, G_T, L, C, d_u
Output: Ω_u^l, $E_{u,c}^l$, $R_{u,c}^l$, $I_{u,c}^l$, ψ_u^l

1: Initialisation: $k = 0$, $P^k = P_{u,c}^l = P/C$
2: **while** sub-channel allocation changes **do**
3:     $u^k(c) = \max_{u \in \mathcal{U}} \ b_{u,c}^l \log_2 \left(1 + \frac{P_{u,c}^l |h_{u,c}^l|^2(t)}{N_0 I_{u,c}^l(t)}\right), \forall c \in \mathcal{C}$
4:     solve the optimization problem in (15)
5:     $k = k + 1$
6: **end while**
7: (u^{k-1}, p^k) is an optimal power allocation

environment with 4G and 5G Radio Access Technologies
(RATs) as umbrella cells with coverage radius ranging from
50m to 500m. Moreover, network users are randomly dis-
tributed across the coverage area and each user's EI and SAR is
evaluated separately. Specifically, in this work, the respective
APs and UEs radiations contribute to a user's EI and SAR
value. The simulation parameters are presented in Table I.

TABLE I
SIMULATION PARAMETERS AND VALUES

Parameters	4G. Values	5G. Values
Number of users	$[10,20,\cdots 60]$	$[10,20,\cdots 60]$
Number of APs	3	3
Channel Model	3GPP	3GPP
Spectrum allocation	20MHz	100MHz
Carrier frequency	2GHz	6GHz
Number of subcarriers per RB	12	12
Size of subcarrier	15KHz	30KHz
RB bandwidth size	12*15=180KHz	360KHz
Number of available RBs	100	250
Tissue's conductivity (σ_u)	0.95S/m	0.97S/m
Mass density of tissue (ρ_u)	1000Kg/m^3	1000Kg/m^3
Characteristic impedance η_0	$120\pi = 377\Omega$	$120\pi = 377\Omega$
Max. AP Tx. power	20W $\approx$ 43dBm	0.25W $\approx$ 24dBm
Max. UE Tx. power	0.25W $\approx$ 24dBm	0.25W $\approx$ 24dBm
Power control	Open-loop	Open-loop
Path loss compensation factor α	0.7	0.7
Slot duration	0.5ms	0.5ms
Scheduling frame	10ms	1ms
Users' distribution	Uniform	Uniform
Antenna height	50m	30m
Height of user device	1.5m	1.5m
Cell coverage radius	500m	30m
Data rate R_u^{min}	2.5Mbps	2.5Mbps
P_{ref}	1W	1W
Tolerable interference, I_u^{max}	-116dBm	-116dBm
Noise spectral density, N_o	10^{-13}W/Hz	10^{-13}W/Hz
Shadow fading	8dB	8dB

A. Impact of Sum Tolerable Network Interference

Figure 3 shows the impact of a network's user per AP on
the overall network tolerable interference for the proposed EI
power-controlled scheme and the conventional 5G network.
In Fig. 3, we consider a scenario in which we vary the
number of users per AP from 10 to 60 for a network with
a coverage radius set at 50m, 75m, and 100m, respectively.
We observe that, as the number of users increases, the net-
work's tolerable interference increases for both the EI power
controlled scheme and the conventional 5G network scheme.
In addition, we observe that the proposed EI demonstrated
promising outcomes with a notable decrease in the network's
overall tolerated interference, which is lower when compared
with the interference limit of -116dBm (i.e., 2.5×10^{-15}W).
This is because an optimized EI further controls the UL and
DL transmit power, which in turn lowers the interference
levels. Simply put, reducing RF-EMF radiation results in lower
levels of interference in the network.

B. Impact of Power Density

In Fig. 4, we present the impact of the power density on the
network. We consider network scenarios in which the number
of users per AP is varied from 10 to 60 and the coverage
radius of the environment is set at 50m, 75m, and 100m,
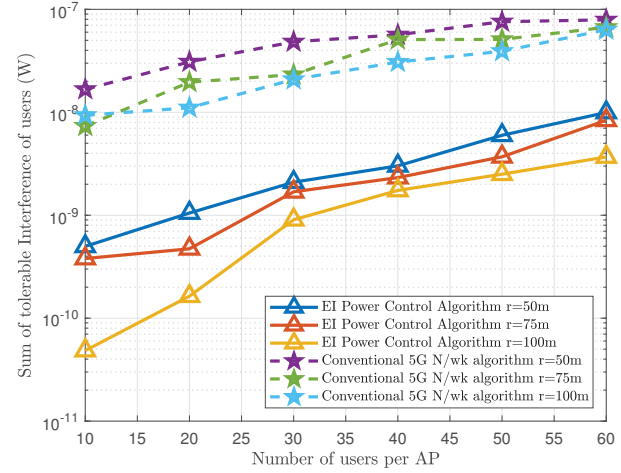similar to the scenario in section VI-A. We see an increase in

Fig. 3. Effect of the number of users per AP on the tolerable interference
for both the EI power controlled scheme and conventional 5G for respective
coverage radius.

the power density of the network as the number of users per
AP increases. Furthermore, we discovered that the proposed EI
power control scheme outperformed the conventional scheme
across the board. The higher the density of the mobile network
environment, the greater the radiation exposure to network
users. Therefore, since the EI power control scheme is ob-
served to have a power density which is less than the threshold
of 10W/m^2 recommended by the United States (US) Federal
Communications Commission (FCC), the network users will
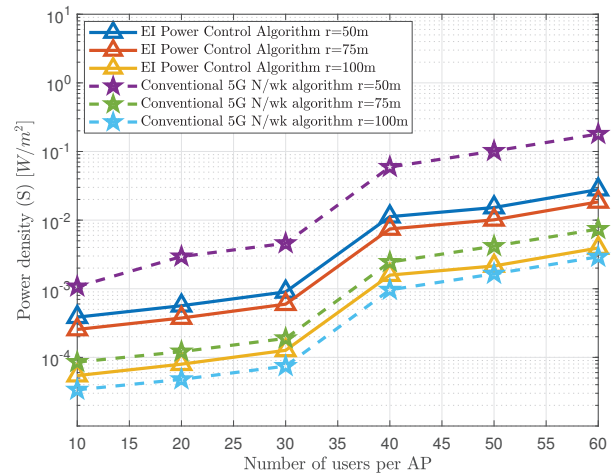experience less radiation exposure.

Fig. 4. Effect of the number of users per AP on the network's power density
for both the EI power controlled scheme and conventional 5G for respective
coverage radius.

C. Impact of Data Rate Threshold on Users

Setting the data rate threshold is a means of ensuring QoS
for network users. In Fig. 5, we set the data rate threshold
to 2.5Mbps and then examine its impact on the network's
average EI. Figure 5 shows that both schemes meet the

QoS threshold requirement. However, the conventional scheme provides higher data rates to network users. Additionally, a closer look at Fig. 5 reveals that the proposed scheme meets the QoS requirement (i.e., data rate threshold) with a minimal average EI value. This is owing to its main goal of minimizing EI while also meeting the QoS requirement. Hence, it ensures the minimum transmit power is used to minimize EI while also meeting the QoS constraints.
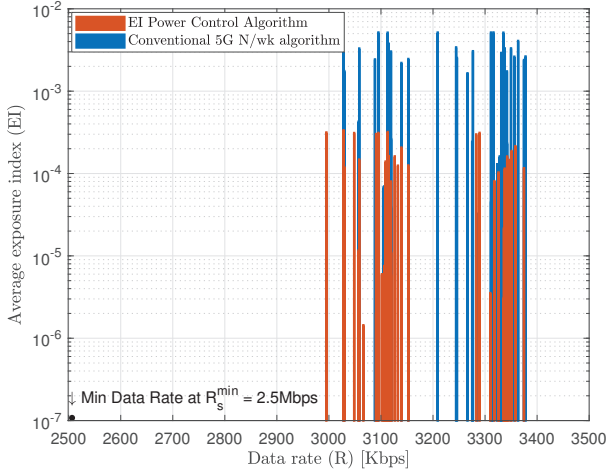

Fig. 5. Effect of data rate threshold as a QoS metric on the network's average EI for both the EI power controlled and conventional 5G schemes.

D. The Effect of the Path Loss Compensation Factor

We explore the impact of the path loss compensation factor on the power density and the average SAR of users of the network in Fig. 6 and Fig. 7.

Fig. 6 presents the effect of the path loss compensation factor α on the network's power density. Herein, α is set at 0.5, 0.7, and 0.9, to examine the performance of the network. We observe that the power density increases as α for both schemes. However, the proposed scheme exhibits a lower power density value for all the set values of α.

In Fig. 7, the effect of the sum of users per AP on the network's average SAR of users with respect to α is set at the specific values of 0.5, 0.7, and 0.9, respectively. As the number of users per AP increases, we observe that the average SAR of users also increases, though it is still below the threshold of 0.08W/Kg advised by ICNIRP. We also observe that for both schemes and for a defined number of users per AP, Fig. 7 shows that the average SAR increases as α increases.

E. Impact of the Number of Users

We examine the effect of increasing the number of users per AP on the average EI for UL and DL scenarios. Unlike in Figs. 3 to 7, in Fig. 8, we compare the 4G and 5G networks. In Fig. 8, we observe that the network's average EI increases as the number of users per AP increases for all the scenarios. In accordance with the literature, we see that the network's average EI is greater for DL than for UL scenarios for both 4G and 5G networks. This seeming disparity in average EI for
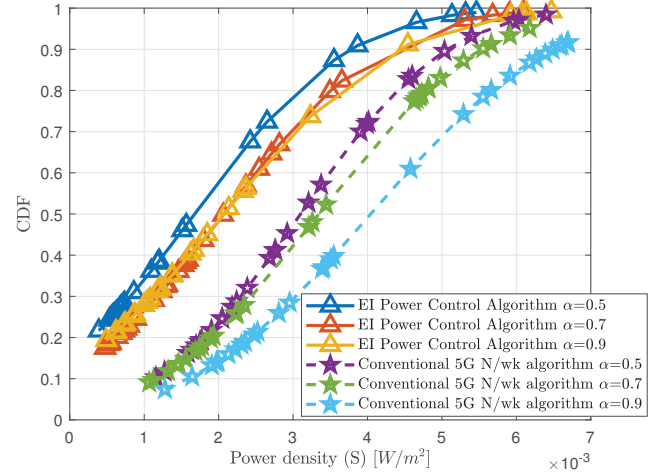

Fig. 6. Impact of the path loss compensation factor on the network's power density for both the EI power controlled and conventional 5G schemes.
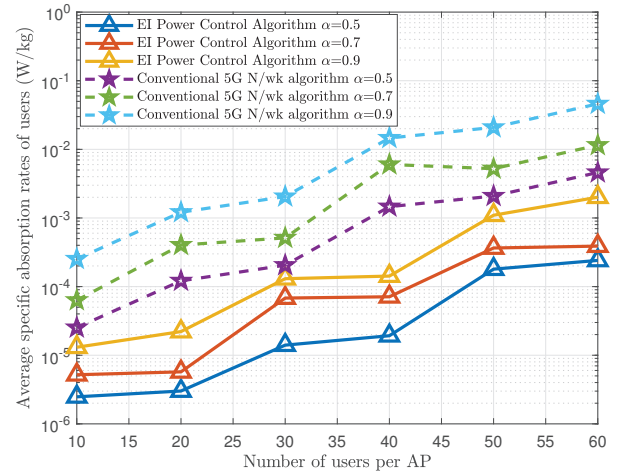

Fig. 7. Impact of the path loss compensation factor on the network's average SAR of users for both the EI power controlled and conventional 5G schemes.

DL and UL scenarios is owing to the higher transmit powers of the APs in the DL transmission. Additionally, we observe that for 5G networks, there is no significant difference between the average EI for UL and DL transmissions for numbers of users per AP less than 10.

F. Impact of the Exposure Duration

Figure 9 presents the impact of the exposure duration on the specific absorption rates of networks on the one hand and also on the network's EI.

In Fig. 9, we observe a direct proportionality in the exposure duration to the network's SAR and EI values. It is noted that as the exposure duration of users on the UE increases, so does the SAR and EI, and this may be harmful to human health. A careful inspection of Fig. 9 reveals that the proposed EI power control scheme exhibits lesser SAR and EI values in comparison to the conventional 5G scheme.
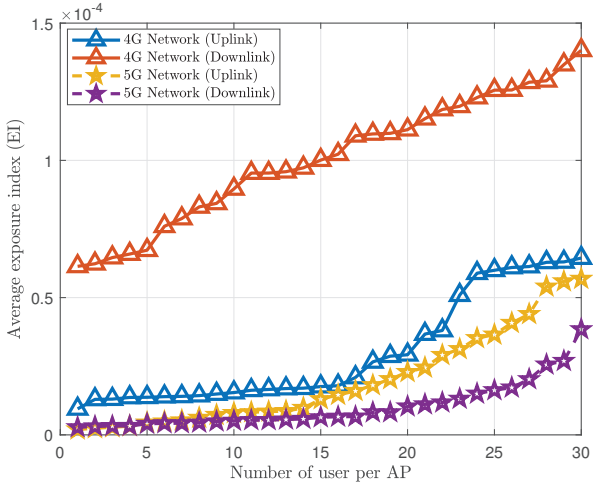
Fig. 8. Impact of the number of users per AP on the network's average EI rates for both 4G and 5G networks in UL and DL scenarios.
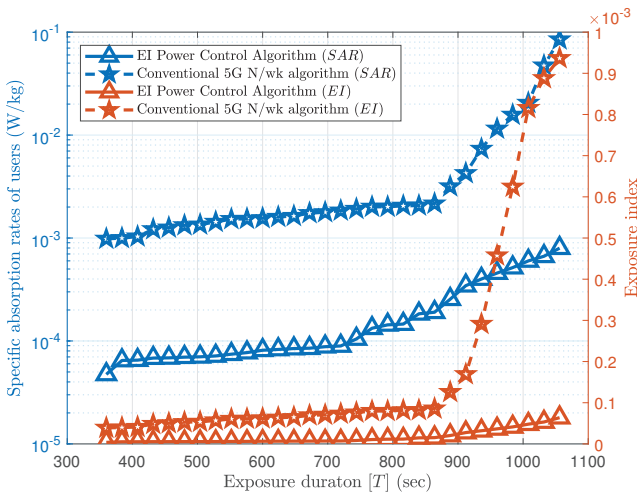

Fig. 9. Impact of the exposure duration on the network's SAR and EI values.

G. Impact of Electric Field Minimisation on Users' Data Rates

The average data rates of users in the network are significantly related to the electric fields generated in the entire network. Both are a function of the transmit power of both uplink and downlink transmissions. With the need to generate more data for the users in the network, the electric field in the network increases. Figure 10 shows the effect of an increased data rate on the total electric field in the network in a scenario where we vary the antenna height to 25m, 50m, and 75m, respectively. In Fig. 10, we observe that the E-fields increase with the average data rate for both the EI power-controlled scheme and the conventional 5G network scheme. We see that the proposed EI showed promising results with a significant reduction in the network's E-fields. Worthy of note is the effect of the antenna's height on the network's electric field; the higher the height, the lower the E-field. Lastly, the propagated E-fields are below the standard threshold of 27.5V/m advised by IEEE Std. C95.1 [66] and ICNIRP [15] for the used
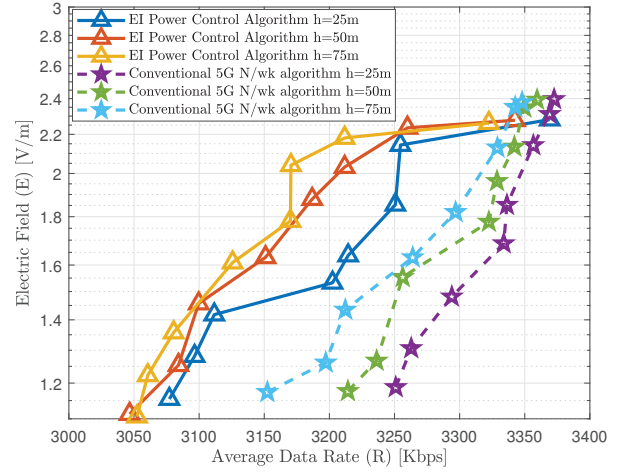
frequency range.

Fig. 10. Illustration of the impact of EI's minimization of the users' data rates.

H. Impact of Power Control on EI

In Figs. 11-14, the average EI caused by the APs and UEs was evaluated for the 4G and 5G networks using their transmit powers and different path loss compensation factors $\alpha = 0.5, 0.7, 0.8,$ and 1, respectively. The downlink power transmit was below the (0.25W) 24dBm for 5G gNBs and below $(20W)$ 43dBm for 4G eNBs, respectively, while the uplink signaling power limit of the UEs was set at (0.25W) 24dBm. Fig. 14 illustrates how the path loss compensation component affects the EI with the full power control compensation of $\alpha = 1$ having the highest average EI compared to fractional power control schemes (where both the cell-edge and cell-center users are accounted for) in Figs. 11-13. It is also evident from Figs. 11-14 that the exposures from the APs (gNBs) are, with the exception of the eNBs, lower than that of the UEs (despite transmitting with more power). This is because these APs are at a farther distance from the users compared to the UEs. Thus, power densities reduce with distance, as supported by the path loss and inverse square law theories.

In addition, it is evident from the findings that 5G networks' exposure doses are lower than those of 4G networks. Among the causes of this include the 5G network's usage of a higher frequency band, which limits the coverage area and, consequently, the radiation exposure. Also worthy of note is that the threshold of the EI is derived to be $10^0 = 1$ [62], based on the standard ERLs. All the 4G and the 5G networks' EIs are observed to be less than this, as depicted in Figs. 11-14 for both whole-body and the local RF-EMF exposures.

I. Impact of SINR on radiation exposure

SINR is a metric that quantifies the quality of a wireless communication link, which indicates the ratio of the desired signal power to the combined interference and noise power. The SINR value is affected by network parameters, such as
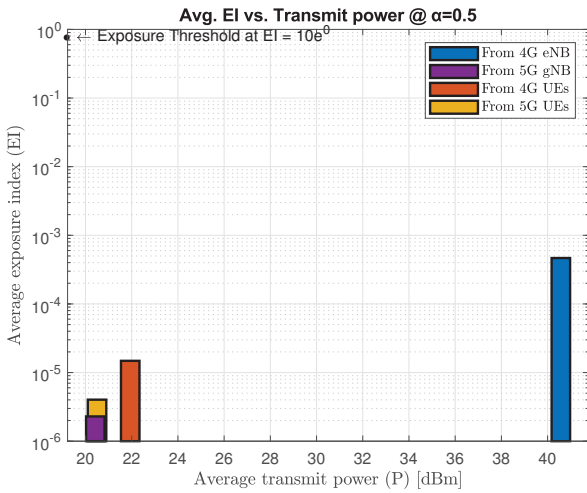
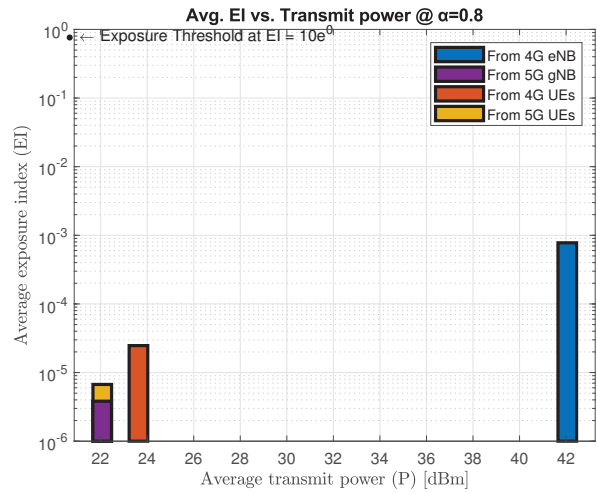Fig. 11. Average EI vs. average transmit power for path loss compensation factor, $\alpha = 0.5$.

Fig. 13. Average EI vs. average transmit power for path loss compensation factor, $\alpha = 0.8$.

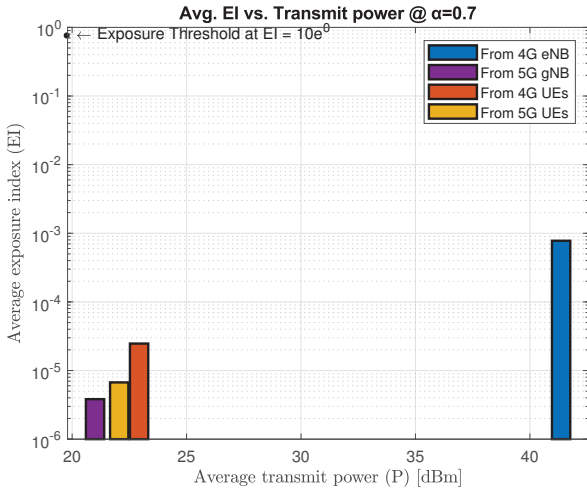
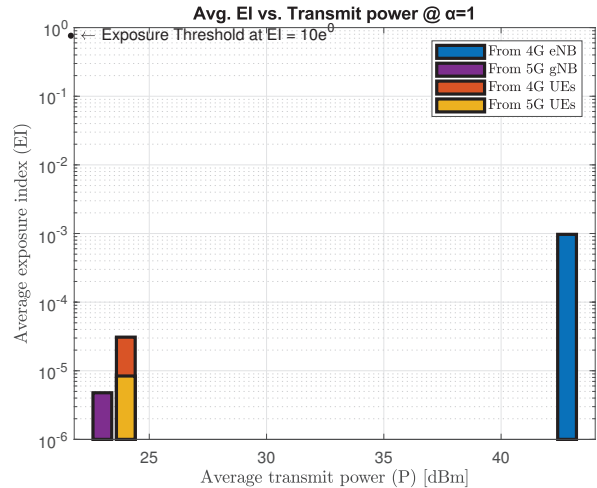Fig. 12. Average EI vs. average transmit power for path loss compensation factor, $\alpha = 0.7$.

Fig. 14. Average EI vs. average transmit power for path loss compensation factor, $\alpha = 1.0$.

signal strength, interference, fading, and noise in the communication channel. However, SAR depends on the power emitted by the wireless, its proximity, and its exposure to the body. In this work, we further explore the impact of the SINR on the network's SAR in Figs. 15, 16, and 17.

In Fig. 15, we present the impact of the SINR on the SAR of network users via the use of conventional 5G networks and the EI power control algorithms. In Fig. 15, the SINR threshold is varied from a 20dB to 35dB range, while setting the power control factor, α, for both algorithms at 0.5, 0.7, and 0.9, respectively. We observed that as the SINR threshold increases, the SAR of users also increases. Additionally, we see that the SARs values are much lower in the proposed EI power control algorithm, which indicates controlled and optimized power when compared with our benchmarked algorithm, the conventional 5G network. Moreover, higher SINR values connote better signal quality and reduced interference, which translates to higher data rates and fewer transmission errors or bit error

rates (BER) if using the modulation technique.

Similar to Fig. 15, Fig. 16 shows the impact of the SINR values on the average EI of the network. In Fig. 16, we vary the SINR threshold range from 20dB to 35dB. We observe that the proposed EI algorithm showed promising EI values which are way lower when compared with the benchmarked algorithm while ensuring the SINR QoS is satisfied.

J. Impact of SINR on power density and transmit power

Figure 17 identifies the trends and the trade-offs between power, power density, and SINR in wireless networks. In Fig. 17, we compare the SINR threshold with the power density and the transmit power in the network. The result shows that the power and the power per unit area values are less in the EI power control algorithm. The power densities of both algorithms provide insight into how power is distributed spatially, which is important for understanding the SAR and EI in the network environment. Additionally, we observe that
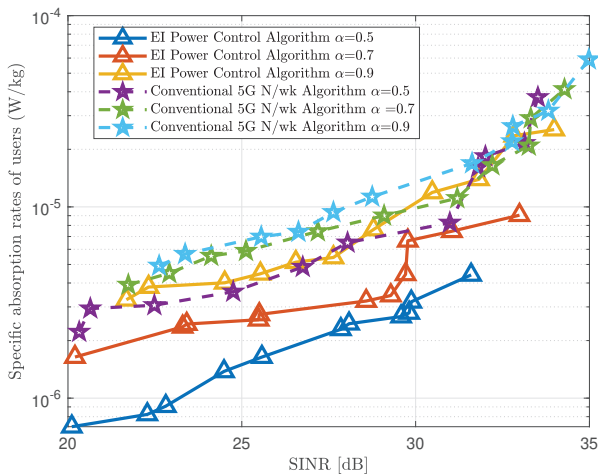
Fig. 15. Impact of the SINR on the SAR of network users for the conventional 5G network and the EI power control algorithms.

Fig. 17. Illustration of the SINR threshold with the power density and the transmit power in the network using the conventional 5G network and the EI power control algorithms.
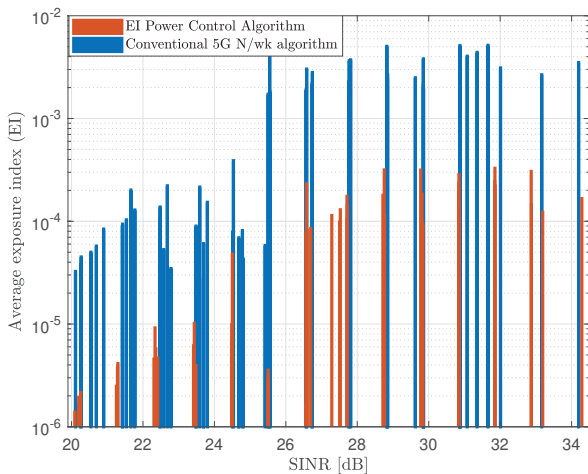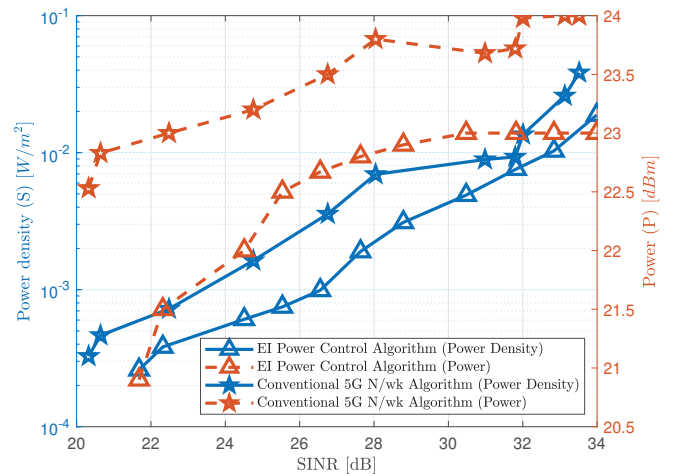

Fig. 16. Impact of the SINR values on the average EI of the network using the conventional 5G network and the EI power control algorithms.

beyond the $23\,\mathrm{dBm}$ power level, additional increases in power may not significantly improve the SINR. This is due to factors such as propagation limitations, interference, or noise.

In Figs. 15-17, we observed that the proposed EI power control algorithm outperforms the benchmarked scheme owing to the network interference being minimized in the proposed EI scheme, as confirmed by the result in Fig. 3. Likewise, the signals from our proposed scheme are higher, as shown in data rates of users in Figs. 5 and 10. The EI power control algorithm has optimized the network parameters using power control and interference management to improve SINR and overall network performance while adhering to SAR and EI safety regulations.

VII. CONCLUSION

In this paper, we have investigated the impact of RF-EMF exposure resulting from wireless networks. We have developed a cutting-edge simulation technique that evaluates the uplink and downlink electromagnetic-field radiation exposures on users of both 5G and 4G networks. With the introduction of a power control model to the networks, the EI was evaluated using the power density, electric field, magnetic field, and SAR, as well as the tissue's conductivity and density. We further developed a power control algorithm that minimizes the exposure in the networks. Using MINLP, we minimized the UL and DL RF-EMF exposures emitted to the users within the network by considering the data rate, power, and interference limits as the QoS constraints.

The proposed scheme was simulated using MATLAB, and the results of our numerical analysis were compared to the other simulated algorithms based on the standards set by regulatory bodies such as the FCC, IEEE, and ICNIRP, to determine the level of compliance and the exposure impact. The evaluation confirmed that the exposures are far lower than the recommended limits and that the exposures are minimized without compromising the users' QoS. Moreover, via the simulation, we compared the EI emitted from the 5G networks and the 4G networks. The results compared the radiation from the UL and DL transmissions in both the 5G and the 4G mobile networks. In a multi-domain environment, that is, an EMF environment with multiple mobile network operators, the total number of UEs and BS is large. To replicate this with a single mobile network, we have increased the number of BS and UEs; hence, we have a dense network. Moreover, in future work, we shall address a multi-domain environment in-depth. We also plan to study and compare the RF-EMF exposure impacts of the C-band frequency range with the millimeter-wave frequency band.

## REFERENCES

[1] Cisco, "Cisco Visual Networking Index: Forecast and trends, 2017–2022 white paper," *Technical Report*, 2019.

[2] U. Uyoata, J. Mwangama, and R. Adeogun, "Relaying in the internet of things (IoT): A survey," *IEEE Access*, vol. 9, pp. 132 675–132 704, 2021.

[3] S. Katsumata, T. Ichikohji, S. Nakano, S. Yamaguchi, and F. Ikuine, "Changes in the use of mobile devices during the crisis: Immediate response to the COVID-19 pandemic," *Computers in Human Behavior Reports*, p. 100168, 2022.

[4] S. Mendonça, B. Damásio, L. C. de Freitas, L. Oliveira, M. Cichy, and A. Nicita, "The rise of 5G technologies and systems: A quantitative analysis of knowledge production," *Telecommunications Policy*, vol. 46, no. 4, p. 102327, 2022.

[5] B. Aghoutane, S. Das, M. E. Ghzaoui, B. Madhav, and H. El Faylali, "A novel dual band high gain 4-port millimeter wave MIMO antenna array for 28/37 ghz 5G applications," *AEU-International Journal of Electronics and Communications*, vol. 145, p. 154071, 2022.

[6] N. M. Kibinda and X. Ge, "User-centric cooperative transmissions-enabled handover for ultra-dense networks," *IEEE Transactions on Vehicular Technology*, vol. 71, no. 4, pp. 4184–4197, 2022.

[7] L. Chiaraviglio, A. Elzanaty, and M.-S. Alouini, "Health risks associated with 5G exposure: A view from the communications engineering perspective," *IEEE Open Journal of the Communications Society*, vol. 2, pp. 2131–2179, 2021.

[8] F. T. Materia, K. Faasse, and J. M. Smyth, "Understanding and preventing health concerns about emerging mobile health technologies," *JMIR mHealth and uHealth*, vol. 8, no. 5, p. e14375, 2020.

[9] M. A. Jamshed, F. Heliot, and T. W. Brown, "A survey on electromagnetic risk assessment and evaluation mechanism for future wireless communication systems," *IEEE Journal of Electromagnetics, RF and Microwaves in Medicine and Biology*, vol. 4, no. 1, pp. 24–36, 2019.

[10] A. Di Ciaula, "Towards 5G communication systems: Are there health implications?" *International Journal of Hygiene and Environmental Health*, vol. 221, no. 3, pp. 367–375, 2018.

[11] L. Verhey and P. Petti, "Principles of radiation physics," *Textbook of Radiation Oncology*, vol. 6, pp. 101–127, 1998.

[12] J. Hannig and R. C. Lee, "Structural changes in cell membranes after ionizing electromagnetic field exposure," *IEEE Transactions on Plasma Science*, vol. 28, no. 1, pp. 97–101, 2000.

[13] International Commission on Non-Ionizing Radiation Protection and others, "Principles for non-ionizing radiation protection," *Health Physics*, vol. 118, no. 5, pp. 477–482, 2020.

[14] ——, "Guidelines for limiting exposure to time-varying electric, magnetic, and electromagnetic fields (up to 300 ghz)," *Health Physics*, vol. 74, no. 4, pp. 494–522, 1998.

[15] ——, "Guidelines for limiting exposure to electromagnetic fields (100 khz to 300 ghz)," *Health Physics*, vol. 118, no. 5, pp. 483–524, 2020.

[16] G. Vermeeren, D. Plets, W. Joseph, L. Martens, C. Oliveira, D. Sebastião, M. Ferreira, F. Cardoso, L. Correia, M. Koprivica *et al.*, "Low EMF exposure future networks d2. 8 global wireless exposure metric definition," *LEXNET Consortium, Moulineaux, France, Tech. Rep. D*, vol. 2, 2015.

[17] A. T. Ajibare and D. Ramotsoela, "A radiofrequency electromagnetic wave radiation exposure minimization method in 5g network: A perspective of qos trade offs," in *2021 International Conference on Electrical, Computer and Energy Technologies (ICECET)*. IEEE, 2021, pp. 1–6.

[18] C. L. Russell, "5G Wireless telecommunications expansion: Public health and environmental implications," *Environmental Research*, vol. 165, pp. 484–495, 2018.

[19] A.-K. Lee and H.-D. Choi, "Brain EM exposure for voice calls of mobile phones in wireless communication environment of Seoul, Korea," *IEEE Access*, vol. 8, pp. 163 176–163 185, 2020.

[20] E. Conil, Y. Corre, N. Varsier, A. Hadjem, G. Vermeeren, W. Joseph, S. Aerts, D. Plets, L. Martens, L. M. Correia *et al.*, "Exposure index of EU project LEXNET: Principles and simulation-based computation," in *8th European Conference on Antennas and Propagation (EUCAP 2014)*. IEEE, 2014, pp. 3029–3032.

[21] I. O. Elujide, O. O. Olugbara, P. Owolawi, and T. Nepal, "Performance of the local averaging handover technique in long term evolution networks," *SAIEE Africa Research Journal*, vol. 106, no. 4, pp. 212–220, 2015.

[22] P. Mishra, P. Thakur, and G. Singh, "Sustainable smart city to society 5.0: State-of-the-art and research challenges," *SAIEE Africa Research Journal*, vol. 113, no. 4, pp. 152–164, 2022.

[23] E. K. Chemweno, P. Kumar, and T. J. Afullo, "Substrate integrated waveguide-dielectric resonator antenna for future wireless communication," *SAIEE Africa Research Journal*, vol. 113, no. 3, pp. 119–128, 2022.

[24] S. O. Oladejo, S. O. Ekwe, and L. A. Akinyemi, "Multi-tier multi-domain network slicing: A resource allocation perspective," in *2021 IEEE AFRICON*, 2021, pp. 1–6.

[25] S. O. Ekwe, L. A. Akinyemi, S. O. Oladejo, and N. Ventura, "Social-aware joint uplink and downlink resource allocation scheme using genetic algorithm," in *2021 IEEE AFRICON*, 2021, pp. 1–6.

[26] S. O. Ekwe, S. O. Oladejo, L. A. Akinyemi, and N. Ventura, "A socially-inspired energy-efficient resource allocation algorithm for future wireless network," in *2020 16th International Computer Engineering Conference (ICENCO)*, 2020, pp. 168–173.

[27] S. Oladejo and O. Falowo, "An energy-efficient resource allocation scheme for 5G slice networks," in *Proc. Southern Afr. Telecommun. Netw. Appl. Conf.*, 2019, pp. 1–4.

[28] S. O. Oladejo and O. E. Falowo, "Latency-aware dynamic resource allocation scheme for 5G heterogeneous network: A network slicing-multitenancy scenario," in *2019 International Conference on Wireless and Mobile Computing, Networking and Communications (WiMob)*, 2019, pp. 1–7.

[29] S. O. Oladejo, S. O. Ekwe, and L. A. Akinyemi, "Multi-tier multi-tenant network slicing: A multi-domain games approach," *ITU Journal on Future and Evolving Technologies*, vol. 2, no. 6, 2021.

[30] Z. Dong, J. Wei, X. Chen, and P. Zheng, "Energy efficiency optimization and resource allocation of cross-layer broadband wireless communication system," *IEEE Access*, vol. 8, pp. 50 740–50 754, 2020.

[31] K. Karipidis, R. Mate, D. Urban, R. Tinker, and A. Wood, "5G mobile networks and health— A state-of-the-science review of the research into low-level RF fields above 6 ghz," *Journal of Exposure Science & Environmental Epidemiology*, vol. 31, no. 4, pp. 585–605, 2021.

[32] H. Hinrikus, T. Koppel, J. Lass, H. Orru, P. Roosipuu, and M. Bachmann, "Possible health effects on the human brain by various generations of mobile telecommunication: A review based estimation of 5G impact," *International Journal of Radiation Biology*, pp. 1–12, 2022.

[33] T. Brown, "Containing exposure in 5G networks, a perspective from LExNet," in *5G Radio Technology Seminar. Exploring Technical Challenges in the Emerging 5G Ecosystem*, 2015, pp. 1–13.

[34] B. Awada, G. Madi, A. Mohsen, A. Harb, A. Diab, L. Hamawy, H. Hajj-Hassan, and M. Hajj-Hassan, "Simulation of the effect of 5G cell phone radiation on human brain," in *2018 IEEE International Multidisciplinary Conference on Engineering Technology (IMCET)*, 2018, pp. 1–6.

[35] F. Kaburcuk, A. Z. Elsherbeni, R. Lumnitzer, and A. Tanner, "SAR and temperature distributions in a head model due to electromagnetic radiation with frequencies up to 100 ghz," in *2020 IEEE International Symposium on Antennas and Propagation and North American Radio Science Meeting*, 2020, pp. 1309–1310.

[36] S. Hannan, M. T. Islam, M. S. Soliman, M. R. I. Faruque, N. Misran, M. Islam *et al.*, "A co-polarization-insensitive metamaterial absorber for 5G n78 mobile devices at 3.5 GHz to reduce the specific absorption rate," *Scientific Reports*, vol. 12, no. 1, pp. 1–13, 2022.

[37] T. Ramachandran, M. R. I. Faruque, A. M. Siddiky, and M. T. Islam, "Reduction of 5G cellular network radiation in wireless mobile phone using an asymmetric square shaped passive metamaterial design," *Scientific Reports*, vol. 11, no. 1, pp. 1–22, 2021.

[38] Y. Huang and J. Wiart, "Simplified assessment method for population RF exposure induced by a 4G network," *IEEE Journal of Electromagnetics, RF and Microwaves in Medicine and Biology*, vol. 1, no. 1, pp. 34–40, 2017.

[39] Z. Kaijage and M. Kissaka, "Assessment of radio-frequency radiation exposure levels: A case of selected mobile base stations in Dar es Salaam, Tanzania," in *2018 IST-Africa Week Conference (IST-Africa)*, 2018, pp. Page 1 of 8–Page 8 of 8.

[40] P. Mandl, P. Pezzei, and E. Leitgeb, "Selected health and law issues regarding mobile communications with respect to 5G," in *2018 International Conference on Broadband Communications for Next Generation Networks and Multimedia Applications (CoBCom)*, 2018, pp. 1–5.

[41] P. Joshi, D. Colombi, B. Thors, L.-E. Larsson, and C. Törnevik, "Output power levels of 4G user equipment and implications on realistic RF EMF exposure assessments," *IEEE Access*, vol. 5, pp. 4545–4550, 2017.

[42] E. Dahlman, S. Parkvall, and J. Skold, *4G, LTE-Advanced Pro and The Road to 5G*, 3rd ed. 125 London Wall, London EC2Y 5AS, United Kingdom: Academic Press, 2016.

[43] C. Törnevik, T. Wigren, S. Guo, and K. Huisman, "Time averaged power control of a 4G or a 5G radio base station for RF EMF compliance," *IEEE Access*, vol. 8, pp. 211 937–211 950, 2020.

[44] S. Okuyucu, K. Yeğın, M. Seçmen, and B. Özbakış, "Parametric SAR study for 4G cellular phone applications," in *2018 22nd International Microwave and Radar Conference (MIKON)*, 2018, pp. 308–311.

[45] G. Koutitas and T. Samaras, "Exposure minimization in indoor wireless networks," *IEEE Antennas and Wireless Propagation Letters*, vol. 9, pp. 199–202, 2010.

[46] M. A. Jamshed, F. Heliot, and T. W. Brown, "Unsupervised learning based emission-aware uplink resource allocation scheme for non-orthogonal multiple access systems," *IEEE Transactions on Vehicular Technology*, vol. 70, no. 8, pp. 7681–7691, 2021.

[47] A. Gati, E. Conil, M.-F. Man-Faï Wong, and J. Wiart, "Duality between uplink local and downlink whole-body exposures in operating networks," *IEEE Transactions on Electromagnetic Compatibility*, vol. 52, no. 4, pp. 829–836, 2010.

[48] T. Sarrebourse, L. R. de Lope, A. Hadjem, L. F. Diez, S. M. Anwar, R. Agüero, Y. Toulain, and J. Wian, "Towards EMF exposure assessment over real cellular networks: An experimental study based on complementary tools," in *2014 11th International Symposium on Wireless Communications Systems (ISWCS)*, 2014, pp. 786–790.

[49] M. Popović, M. Tesanovic, and B. Radier, "Strategies for reducing the global EMF exposure: Cellular operators perspective," in *2014 11th International Symposium on Wireless Communications Systems (ISWCS)*, 2014, pp. 836–841.

[50] J. Stephan, M. Brau, Y. Corre, and Y. Lostanlen, "Joint analysis of small-cell network performance and urban electromagnetic field exposure," in *The 8th European Conference on Antennas and Propagation (EuCAP 2014)*, 2014, pp. 2623–2627.

[51] Y. A. Sambo, M. Al-Imari, F. Héliot, and M. A. Imran, "Electromagnetic emission-aware schedulers for the uplink of OFDM wireless communication systems," *IEEE Transactions on Vehicular Technology*, vol. 66, no. 2, pp. 1313–1323, 2016.

[52] A. T. Ajibare and O. E. Falowo, "Resource allocation and admission control strategy for 5G networks using slices and users priorities," in *2019 IEEE AFRICON*, 2019, pp. 1–6.

[53] S.-Y. Lien, S.-L. Shieh, Y. Huang, B. Su, Y.-L. Hsu, and H.-Y. Wei, "5G New Radio: Waveform, frame structure, multiple access, and initial access," *IEEE Communications Magazine*, vol. 55, no. 6, pp. 64–71, 2017.

[54] P. Kyosti, "Winner ii channel models," *IST, Tech. Rep. IST-4-027756 WINNER II D1. 1.2 V1. 2*, 2007.

[55] A. Abdelnasser and E. Hossain, "On resource allocation for downlink power minimization in OFDMA small cells in a cloud-ran," in *2015 IEEE Global Communications Conference (GLOBECOM)*, 2015, pp. 1–6.

[56] T. Chrysikos and S. Kotsopoulos, "Rf channel modeling for 5G systems," in *New Directions in Wireless Communications Systems*. CRC Press, 2017, pp. 47–68.

[57] D. Poljak and M. Cvetkovic, *Human Interaction with Electromagnetic Fields: Computational Models in Dosimetry*. Academic Press, 2019.

[58] I. W. G. on the Evaluation of Carcinogenic Risks to Humans *et al.*, "Non-ionizing radiation, part 2: Radiofrequency electromagnetic fields." *IARC monographs on the evaluation of carcinogenic risks to humans*, vol. 102, no. PT 2, p. 1, 2013.

[59] G. Fischer, F. Pivit, and W. Wiebeck, "Link budget comparison of different mobile communication systems based on EIRP and EISL," *Advances in Radio Science*, vol. 2, no. BC, pp. 127–133, 2005.

[60] E. Tejaswi and B. Suresh, "Survey of power control schemes for LTE uplink," *Int Journal Computer Science and Inform Technol*, vol. 10, p. 2, 2013.

[61] A. Haider and S.-H. Hwang, "Maximum transmit power for UE in an LTE small cell uplink," *Electronics*, vol. 8, no. 7, p. 796, 2019.

[62] A. T. Ajibare, D. Ramotsoela, L. A. Akinyemi, and S. O. Oladejo, "Rf emf radiation exposure assessment of 5g networks: Analysis, computation and mitigation methods," in *2021 IEEE AFRICON*, 2021, pp. 1–6.

[63] T. ETSI, "136 101 v12. 7.0 (2015-05): Lte; evolved universal terrestrial radio access (e-utra); user equipment (UE) radio transmission and reception (3gpp ts 36.101 version 14.3. 0 release 14)."

[64] ——, "138 101-1 v17. 5.0. 5g; nr; user equipment (UE) radio transmission and reception; part 1: Range 1 standalone (3gpp ts 38.101-1 version 17.5. 0 release 17)," *Sophia Antipolis Cedex, France: ETSI*, 2022.

[65] H.-W. Lee and S. Chong, "Downlink resource allocation in multi-carrier systems: frequency-selective vs. equal power allocation," *IEEE Transactions on Wireless Communications*, vol. 7, no. 10, pp. 3738–3747, 2008.

[66] IEEE, "IEEE standard for safety levels with respect to human exposure to electric, magnetic, and electromagnetic fields, 0 Hz to 300 GHz," *IEEE Std.*, 2019.
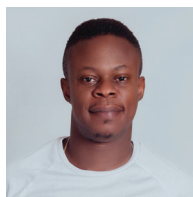
Adedotun T. Ajibare obtained his MSc. in Information Technology and MSc. Eng. in Electrical Engineering from the National Open University of Nigeria, Nigeria and the University of Cape Town, South Africa, respectively. He is currently pursuing a PhD in Electrical Engineering at the University of Cape Town, South Africa. His research interests include 5G networks, radio resource management in wireless networks, network optimization, radiofrequency radiation, data analytics, and computational intelligence.

Sunday O. Oladejo received his PhD in Electrical and Electronic Engineering from the University of Cape Town, South Africa, in 2021. He is currently a postdoctoral research fellow at the School for Data Science and Computational Thinking, Stellenbosch University, South Africa. From 2007 to 2017, he was a Senior Core Network Engineer with Glo-Mobile, Nigeria. His research interests include radio resource management in wireless networks, artificial intelligence, swarm intelligence, optimization, computational thinking, data science and analytics.

Stephen O. Ekwe obtained his B.Eng in Electrical Electronic Engineering in 2008 from the Cross River University of Technology, Calabar, Nigeria, and a Master of Science in Personal, Mobile, and Satellite Communication in 2013 from the University of Bradford, West Yorkshire, England. He is currently pursuing a PhD in Electrical Engineering at the University of Cape Town, South Africa. His research interests include 5G, terrestrial and non-terrestrial communication integration, social-aware networks, network optimization, machine and reinforcement learning, computational intelligence, meta-heuristic optimization, and radio resource management.

Lateef A. Akinyemi (Senior Member, IEEE) received the B.Sc. degree (Hons.) in electronic and computer engineering (computational electronics) and the M.Sc. degree in electronic and computer engineering from Lagos State University, Lagos, Nigeria, the M.Sc. degree in electrical and electronics engineering (communication engineering option) from the University of Lagos, Akoka, Nigeria, and the PhD degree in electrical engineering from the Department of Electrical Engineering, Faculty of Engineering and the Built Environment, University of Cape Town, Western Cape, South Africa. He is a Lecturer, a Researcher, and a Scholar with the Department of Electronic and Computer Engineering, Faculty of Engineering, Lagos State University, Epe campus, Lagos. Currently, he is a postdoctoral research fellow at the University of South Africa, College of Science, Engineering and Technology, School of Engineering and School of Computing, Department of Computer Science and Department of Electrical Engineering, Florida Campus, Johannesburg, South Africa. His research areas are wireless communications, computational electronics, modelling and simulations of quantum-inspired Nano-particles and devices, microwave engineering and antennas, data science, analytics, artificial intelligence-inspired algorithms, computational intelligence and machine learning.

Daniel Ramotsoela (Member, IEEE) received the BEng., MEng., and PhD degrees in computer engineering from the University of Pretoria, in 2013, 2015, and 2020, respectively. He is currently a Senior Lecturer with the Department of Electrical Engineering, University of Cape Town. His research interests include system security, machine learning, and wireless sensor networks, primarily focusing on IoT applications and cyber-physical systems.

CONTENTS PAGE